A REVIEW OF MECHANOCALORIC REFRIGERATION DEVICES FROM 2012 TO 2020

G. L. Foleis[a],
F. C. Colman[a]
and J. C. D. de Oliveira[a]

[a] Universidade Estadual de Maringá
Departamento de Engenharia Mecânica
Pós Graduação em Engenharia Mecânica
Av. Colombo, 5790, Centro de Tecnologia
Bloco 104 Jd. Universitário
CP. 87020-900, Maringá, Paraná, Brasil
gabrielfoleiss@gmail.com

Received: Mar 03, 2022
Revised: Mar 31, 2022
Accepted: Mar 31, 2022

ABSTRACT

Solid-State room temperature refrigeration devices have been reported extensively in the last decades with a focus on magnetocaloric effect materials, a thermal response to an applied magnetic field in a solid refrigerant. Currently, the limitations to generate large magnetic fields needed for better efficiencies have posed a challenge to rival current standard vapor compression cycles. Conventional refrigerants in standard vapor cycles are expected to contribute to global warming close to 25000 $kgCO_{2,eq}$ over the next 100 years. The need to overcome such challenges has driven a search for alternative *i*-caloric effects such as electrocaloric which is the thermal response of the material to the application of an electric field and mechanocaloric, a thermal response to the application of a stress field. Recently, the latter effect is being reported and categorized by the type of stress field applied. They are named elastocaloric for uniaxial stress, barocaloric for isostatic stress, and torsiocaloric for pure shear. Due to its simple stress, elastocaloric regenerators with shape memory alloys (SMA) were reported first. With a design similar to shell-tube heat exchanger with SMA being the shell and tubes while the heat transfer fluids (HTF) flows within the tubes. Promising thermodynamic cycle parameters such as coefficient of performance COP 11.0 with a temperature span of 24.6 K subject to a strain of 4.5% have been achieved with this design. Another device was reported working in a continuous non-regenerative manner with steady state being reached within seconds presented COP of 9.5 and a heat load of 250 W for a temperature span of 10K. As for barocaloric materials some researchers announced that are currently developing devices with these phenomena. Its main challenge is to elaborate a design that allows cyclic isostatic stress application, usually achieved by encapsulating the barocaloric material. One research group presented a study on a simulated active barocaloric regenerator on metal alloys and Acetoxy Silicone Rubber (ASR). The most recent mechanocaloric effect is the torsiocaloric. Two devices for measuring the torsiocaloric effect where presented, one in a batch form and another setup similar to a heat exchanger shell-tube where the tube is the solid-state refrigerant that can be twisted while in direct contact with the HTF flowing on the shell side. Thus, we aim to provide an in-depth analysis of recent studies of mechanocaloric devices describing their working cycles, thermodynamic parameters, HTF circuits and comparing their design choices, and forecast the design of near future mechanocaloric solid-state devices.

Keywords: solid-state refrigeration; mechanocaloric effect; elastocaloric; barocaloric; torsiocaloric

NOMENCLATURE

ASR	Acetoxy Silicone Rubber
COP	Coefficient of Performance
HTF	Heat Transfer Fluid
$\dot{Q}$	Heat transfer, (W)
SMA	Shape Memory Alloy
TEWI	Total Equivalent Warming Impact
T	temperature, °C
$\dot{W}$	power, W

Greek symbols

Δ	Change,
ε	Elongation, %
σ_b	Applied barocaloric pressure, GPa
σ-CE	Mechanocaloric-effect
σ_e-CE	Elastocaloric-effect
σ_b-CE	Barocaloric-effect
σ_t-CE	Torsiocaloric-effect

Subscripts

ad	adiabatic
amb	ambient temperature
CO	Cold
IN	Inlet
max	maximum
min	minimum
ref	refrigeration

INTRODUCTION

Conventional refrigeration systems use refrigerants such as hydrofluorocarbons (HFC), hydrochlorofluorocarbons (HCFC) and chlorofluorocarbons (CFC) with Total Equivalent Warming Impact (TEWI) in a time horizon of 100 years of 28900, 17400 (Papasavva and Moomaw, 1998) and 25000 (Mota-Babiloni et al., 2020) $kgCO_{2,eq}$ respectively when they come in contact with the atmosphere. This scenario has driven the search for alternative technologies that help minimize the TEWI of the refrigeration systems. In this regard, one promising technology is solid-state cooling with zero emissions as it completely eliminates the need for HFC, HCFC and CFC fluids as this technology uses solid refrigerants (Takeuchi and Sandeman, 2015).

A solid that shows a thermal response as a result of an external field change is said to have an *i*-caloric effect, where *i* becomes Magnetocaloric when the applied field is a magnetic field, Electrocaloric for an electric field and Mechanocaloric for a stress field (Imamura *et al.*, 2018). A comprehensive and thru review of cooling devices that use materials with magneto-caloric effect and electrocaloric effect has been elaborated by Greco et al. (2019), and are briefly reviewed. It can be seen that breakthroughs have been made, prototypes were built and tested with this technology with devices working as either rotary or reciprocating with either permanent magnets or electromagnets. Its lessons and limitations were established, such as the need for large magnetic fields and low efficiencies which poses a challenge to rival current standard vapor compression cycles to date. The use of an auxiliary HTF was shown to be inherent to solid-state cooling designs.

Mechanocaloric-effect (σ-CE) is categorized by the type of stress field applied such as elastocaloric σ_e-CE for uniaxial stresses, barocaloric σ_b-CE for isostatic stresses and torsiocaloric σ_t-CE for pure shear as illustrated in Fig. 1.

Our goal in this paper is to provide a consolidated analysis on recent studies of refrigeration devices that use Mechanocaloric-effects describing their working cycles, reported thermodynamic parameters, auxiliary fluids and their circuits.

ELASTOCALORIC DEVICES

Cui *et al.* (2012) presented the thermal response of a 3 mm diameter of a NiTi wires due to the solid-to-solid martensitic phase transformation when imposed an elongation of 8.5%. During stretch, the wire heated adiabatically to ΔT = 25.8 °C and during stretch release of - 17°C. The Material COP was estimated as 2.7 during cooling when assuming that the unloading energy is not recoverable.

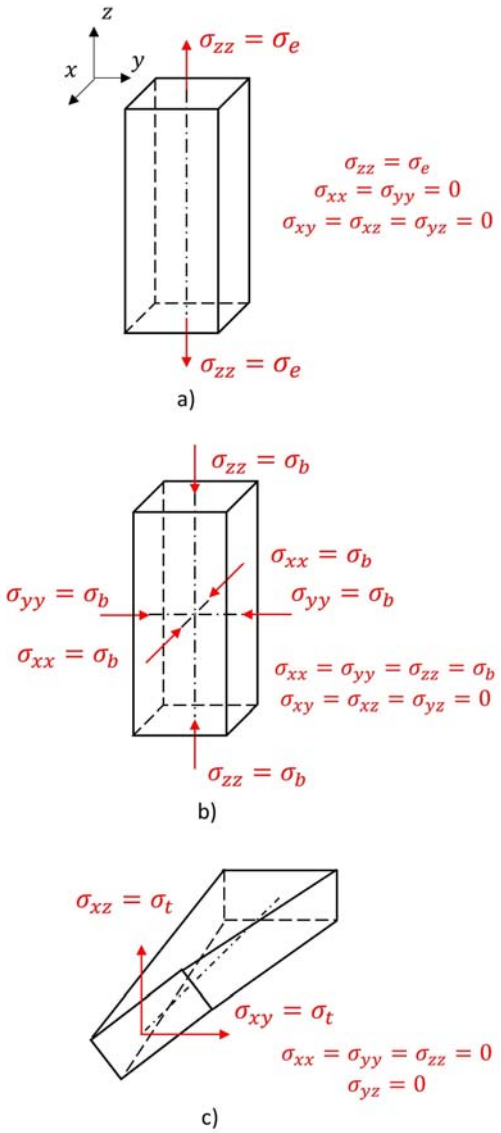

Figure 1. Stress states for: a) Elastocaloric effect b) Barocaloric Effect c) Torsiocaloric Effect. Adapted from (Imamura, 2020)

Tusek *et al.* (2016) presented a working active parallel plate regenerator working as a heat pump as presented in Fig. 2 using $Ni_{55.8}Ti_{44.8}$ plates imposing a maximum elongation of 3.4% in order to reduce material fatigue at a frequency of 0.25Hz. Figure. 2(a) shows the 9 parallel plates clamped on the testing machine that imposes the elongations and fluid flow of water as HTF entering at ambient temperature of 24°C. At steady-state, Fig. 2(b), water leaves the hot side at 33.9°C and the cold side at 19.3 °C. Figure 2(c) is the schematic representation of the cycle during the step where fluid water flows towards the cold heat exchanger (CHEX), where heat is absorbed, causing the cooling effect.

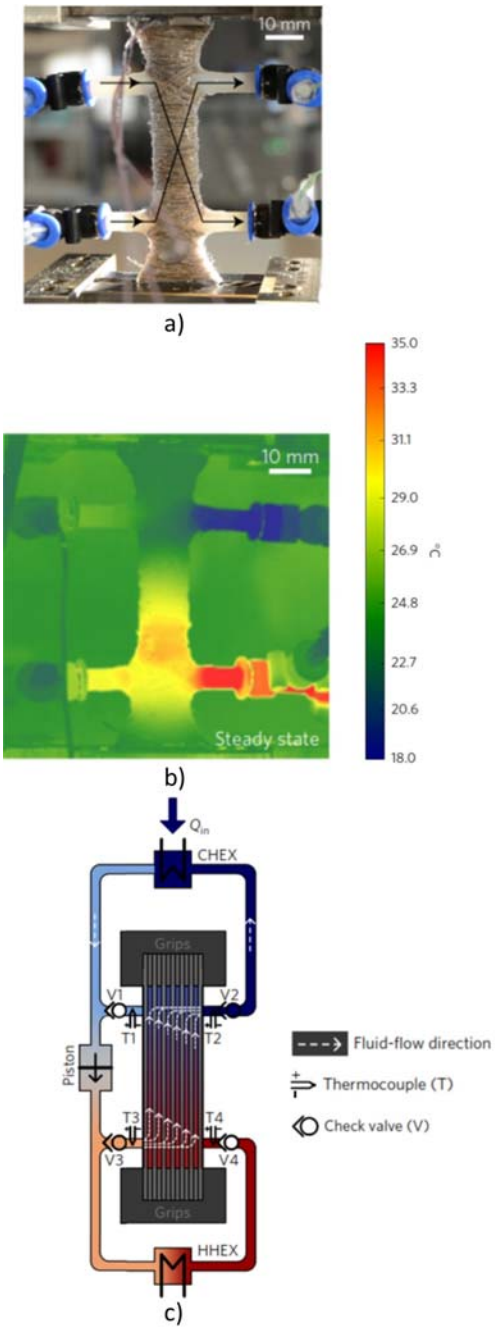

Figure 2. a) Regenerator clamped on the tensile test machine and connected to the fluid loops and its flow directions labeled. b) Thermal distribution at steady state operation after 500 seconds captured with infrared camera c) Illustration of the four step elastocaloric regenerator-based device. Adapted from (Tusek *et al.*, 2016)

Kirsch *et al.* (2018) simulated a continuous rotational device with the goal to be a direct air cooling unit, thus the cool air it achieves is assumed ready to be used and there is no need for additional heat exchanger. Figure 3(a) represents schematically this device outer shell. It measures about 600 mm and has an outer diameter of approximately 300 mm. There are 24 bundles of 30 SMA wires held together utilizing a custom clamp attached in one side to a Tension disk that works as a track, and on the other to the cam track. Additionally, direct air cooling makes for a design with efficient sealing as air is less likely to leak when compared to liquids. The device operates at a frequency of 0.5 Hz utilizing a shape memory alloy, SMA, optimized for caloric cooling $Ti_{55.2}Ni_{29.3}Cu_{12.7}Co_{2.8}$ reaching steady-state operation in 2 seconds with a total mass of SMA of m_{sma} = 50 g providing a cooling power of $\dot{Q}_{ref}$ = 250 W with the driving system mean power required being $\dot{W}_{drive}$ = 25 W resulting in a COP of 9.5.

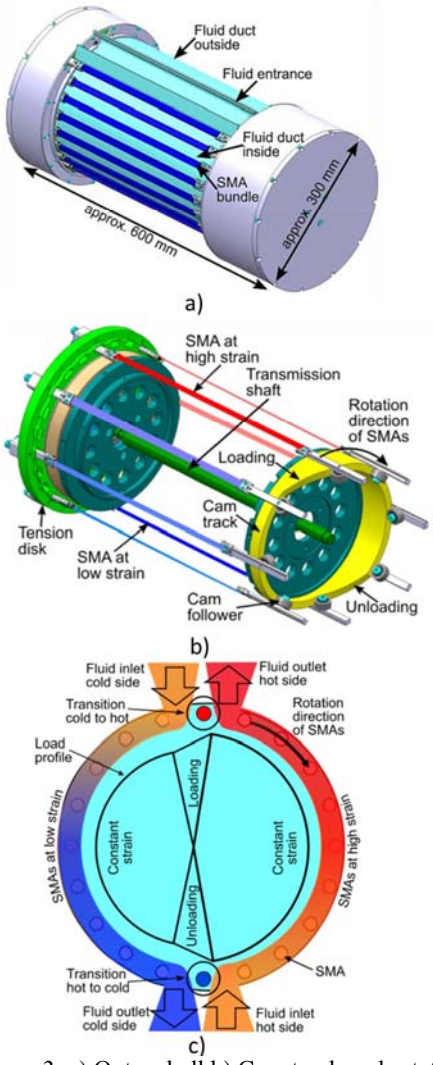

Figure 3. a) Outer shell b) Cam track and rotation direction c) Expected thermal distribution and fluid flow directions. Adapted from (Kirsch *et al.*, 2018)

Figure 3(b) represents schematically this device´s operation. The wires are subject to a controlled deformation, which in turn impose a tensile state shown in red at the first half using a carefully designed Cam track and a removal of this deformation at the second half, shown in blue. It is

important to note that this design makes the work recovery be inherent to its operation minimizing cycle energy input needed, similar to how work is recovered in a Reverse Brayton Cycle (Shapiro and Moran, 2006). The first half is the Loading Phase, an elongation of ε_{max} = 4.5% is imposed causing the wires to heat to 42.3°C due to the elastocaloric effect and is cooled to 24.5°C by air. Upon arriving at the second half there is an Unloading Phase and the elongation is removed and they are cooled by the elastocaloric effect to -4.4°C and, as it cools the air that will carry the cooling load, the SMA heats to 15.9°C. This means that the estimated as $\Delta T_{ad,\varepsilon_{max}}$ = 26.4°C and $\Delta T_{ad,\varepsilon_{min}}$ = -28.9°C. This difference is due to the hysteresis this material has during the phase transformation that generates the elastocaloric effect. It can be seen that the design is trying to minimize the hysteresis effect over the cycle efficiency.

Figure 3(c) shows schematically the expected temperature distribution on a steady-state operation and the air inlet at the cooling side, at a flow rate of 75 m^3/h at ambient temperature $T_{amb} = T_{IN}$ = 20°C and leaves at a refrigerated state at T_{CO} = 9.8°C and flow speed of 8.7 m/s. On the heating side it also enters at the same flow rate and temperature and leaves at 30.1°C.

Aprea *et al.* (2018) developed a generic model of an Active Caloric Regenerative refrigeration cycle, ACR, as a 2D model to analyze an array of *i*-caloric effects materials. Figure 4(a) presents its main components as CHEX Cold Heat Exchanger, ACR - Active Caloric Regenerator, HHEX - Hot Heat Exchanger, Y - External field applied and Pump. Although it is not explained how the external fields could be applied, it assumes that it could and it undergoes a 4 step cycle that for an elastocaloric material would be as follows: 1st step with the HTF still apply an given elongation to the 2D thin plates of σ_e-CE material which heats adiabatically as it is subject to the given stress field. 2nd step pump the HTF from CHEX to HHEX cooling the ACR and in the HHEX let it reject the heat. 3rd step stop the pump and reduce the imposed elongation and consequentially the stress field and the σ_e-CE material cools adiabatically. 4th step turn on the pump and force the HTF to flow from HHEX to the CHEX thru the ACR as it is cooled and it moves the cooling load to the CHEX where it is used.

Figure 4(b) shows schematically the thin layers of σ_e-CE material plates and the HTF channels. The ACR dimensions are height H = 20 mm, its length L = 40 mm, and each plate has a thickness of 0.25 mm while the HTF channels are 0.125 mm thick. Laminar, incompressible non-viscous flow is considered.

The COP is similar for all three tested materials with a mass flow rate per unit area of $\dot{m}/A$ = 250 kg $s^{-1}m^{-2}$ ranging from 8.9 to 11.1, and the applied stress field from 0.14 GPa to 2 GPa as detailed at Tab. 1. Upon inspection of it one could argue that the smaller the stress field the safer the equipment is expected to be, thus $Cu_{68.13}Zn_{15.74}Al_{16.13}$ stress field is more than 14 times smaller than for $PbTiO_3$ and could be a safer choice for a home appliance with higher COP.

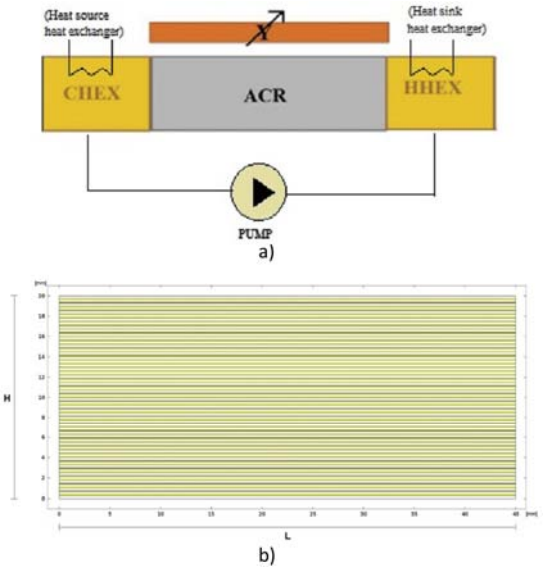

Figure 4. a) CHEX - Cold Heat Exchanger, ACR - Active Caloric Regenerator, HHEX - Hot Heat Exchanger, Y - External field applied and Pump b) 2D thin plates of *i*-caloric effects materials stacked with HTF channels. From (Aprea *et al.*, 2018)

Wang *et al.* (2019) characterized the Material COP defined as the specific cooling to the input of gravimetric mechanical work for Natural Rubber (NR) during stretch release. This specific cooling was determined by estimating the average surface and volume temperature change after the deformation using a thermal camera and the energy needed is obtained by determining the work by integration of the area under the respective tensile test curve. This gave a COP = 3.8, with an average surface temperature change of $\Delta T_{avg,surf}$ = - 12.2°C for a ε_{max} = 600%. A summary of the presented elastocaloric devices research groups and their main parameters were assembled on Tables 1 and respectively.

Table 1. Elastocaloric research groups and types.

#	Research group	Type
I	University of Maryland; & others, USA, (Cui *et al.*, 2012)	Batch
II	Technical University of Denmark; & others, (Tusek *et al.*, 2016)	Active
III	Saarland University; Ruhr Universität Bochum, Germany, (Kirsch *et al.*,2018)	Rotary[a]
IV	University of Salermo; University of Naples, Italy, (Aprea *et al.*, 2018)	Cyclic[a] 4 steps
V	Nankai University, China; & many others (Wang *et al.*, 2019)	Batch

(a) Simulation results

Table 2. Elastocaloric device parameters.

#	Elastocaloric Composition	ε_{max} (%)	$\dot{Q}_{ref}$ (W)	T_{amb} (°C)	COP
I	$Ni_{50}Ti_{50}$	8.5	-	22.6	11.8[a]
II	$Ni_{55.8}Ti_{44.8}$	3.4	-	24	-
III	$Ti_{55.2}Ni_{29.3}Cu_{12.7}Co_{2.8}$	4.5	250	20	9.5
IV	NiTi (0.9 GPa)	-	450	room	11.0
	$Cu_{68.13}Zn_{15.74}Al_{16.13}$ (0.14 GPa)	-	418	room	9.3
	$PbTiO_3$ (2 GPa)	-	170	room	8.9
V	NR	600	-	29.74	3.8[a]

(a) of material during stretch release.

BAROCALORIC DEVICES

Aprea *et al.* (2018) also simulated the device described in the previous section for σ_b-CE materials as solid refrigerant. Similarly, no mention is made on how this could be achieved in respect to the driver design that will impose an isostatic stress state. Notice that this makes this type of material present a higher implementation challenge. Upon inspection of Tables 3 and 4, when comparing the materials it can be seen that the material composition is a key factor on the performance and operation parameters. For instance, when choosing $MnCoGe_{0.99}In_{0.01}$ over $(NH_4)2MoO_2F_4$ the same COP of 10 can be achieved with less than half of the applied stress and similar refrigeration power. In the following year Aprea et al. (2019) proposed a schematic of a barocaloric cooling system applied to a Reverse Brayton-based cycle utilizing the elastomer Acetoxy Silicone Rubber, ASR, as the solid-state refrigerant which is considered as a low-cost, easily available and eco-friendly. In Tab. 4 it is shown the operating parameters for maximum COP at 3.9, considering the width of the regenerator as W = 1 m with flow velocity of .1 m/s, fraction of Cu nanoparticles φ_{Cu} = 10% resulting in $\dot{Q}_{ref}$ = 3200 W. A summary of the presented barocaloric devices and their main parameters were assembled at Tables 3 and 4.

Table 3. Barocaloric research groups and types.

#	Research group	Type
I	University of Salermo; University of Naples, Italy, (Aprea *et al.*, 2018)	Cyclic 4 steps
II	University of Salermo; University of Naples, Italy, (Aprea *et al.*, 2019)	Cyclic 4 steps

Table 4. Barocaloric device parameters.

#	Barocaloric Composition	σ_b (GPa)	$\dot{Q}_{ref}$ (W)	T_{amb} (°C)	COP
I	$MnCoGe_{0.99}In_{0.01}$	0.3	383	room	10.0
	$(NH_4)2MoO_2F_4$	0.9	400	room	10.4
	$(NH_4)2MoO_2F_4$	0.7	350	room	10.0
	$(NH_4)2MoO_2F_4$	0.5	236	room	6.8
II	ASR	0.39	3200	room	3.9

TORSIOCALORIC DEVICES

Wang *et al.* (2019) investigated the torsiocaloric effects on vulcanized NR fibers, NiTi wires, polyethylene (PE) and nylon6 fibers. As is the case for polymeric materials, their fabrication processes have a strong impact on material properties, and were carefully characterized.

The specific cooling energy of h_c for the isometric twisting removal of the NR was estimated utilizing the apparatus as show in Fig. 5(a) with the components: (a)80-step servo motor, (b) torsiocaloric material, (c) polypropylene PP tube with water, (d) e (e) thermocouples measuring water and PP tube temperatures, (f) epoxy resin used for bottom sealing, (g) clamps attaching the torsiocaloric material at the motor and tethering. The material is stretched at the desired ε_{max}, up to 600% for NR and twisted. This causes the material to heat due to both σ_e-CE and σ_t-CE and it is left to cool until reaching thermal equilibrium at room temperature when the PP tube is filled with water also at room temperature. After thermal equilibrium, twist release follows and if any stretch was imposed it will be released in sequence. The temperature decrease is directly measured by the thermocouples and used to calculate h_c.

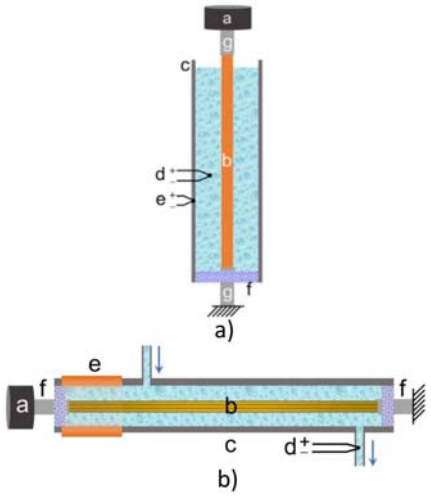

Figure 5. a) Twist and stretch release in batch b) Twist release with flowing water. From (Wang *et al.*, 2019)

A Material COP of 8.5 was obtained for NR with 2.2 mm of diameter with initial length of 3 cm with twist density of 30 turns/cm at T_{amb} = 29.74 °C during a twist removal at a rate of ω = 50 turns/s and stretch release of ε_{max} = 100% at a strain rate of 42 cm/s. With no stretch release, the Material COP drops to 8.3. A single NiTi wire of 0.7 mm diameter was also tested on the device with twist density of 0.8 turns/cm with estimated h_c = 7.9 J g^{-1}.

Figure 5 (b) shows the device used to measure the twist release h_c for 3 plied NiTi wires. It is very similar to the one described previously, except that

the water now flows similar to a single pass shell and tube heat exchanger with the HTF as water on the shell side entering at T_{amb} and the tubes are solid NiTi wires that can be twisted. The components are as follows: (a) 80-step servo motor, (b) NiTi Wires, (c) PP tube with flowing water, (d) thermocouple measuring water exit temperature (e) rubber tube with negligible σ_t-CE, (f) epoxy resin used for sealing the ends, clamps attaching the NiTi wires at the motor and tethering (not labeled) and a peristaltic pump with a constant flow rate (not shown). The plied NiTi wires are twisted and heat due to the σ_t-CE and are cooled by the constant flow of water. After thermal equilibrium is reached the twist release is performed and the temperature decrease is measured and used to estimate h_c. A three-ply NiTi wire 0.6 mm diameter of 11.1 cm long was twisted with Fig.5 (b) with a ω = 0.87 turns/cm cooled by a water flow rate of 0.04 ml/s and h_c = 6.75.

Wang et al. (2020) reported the torsiocaloric material parameters for self-coiling polyvinylidene difluoride (PVDF) fibers. This Material was measured to have COP = 8.8 after a thermal treatment of annealing at 150 °C for 1 hour. With no annealing the COP drops to 2 at ambient temperature.

CONCLUSIONS

As presented in this work, it can be seen that many elastocaloric cooling devices have been investigated and this effect is becoming a well-established mechanocaloric cooling effect and the most promising in the near future. A parallel plate regenerator was built, and simulations of a simple rotary device as well as an alternating parallel plate regenerator were presented. As of the end of 2020, no working barocaloric devices have been published but some simulations were studied for metal alloys and ASR. Two Batch torsiocaloric devices were built and tested experimentally with NR and NiTi wires showing promising results. With the current reports on solid-state refrigeration devices, we see the goal of developing a suitable substitute for vapor compressing cycles closer to becoming reality.

REFERENCES

Aprea, C., Greco, A., Maiorino, A. and Masselli, C., 2018. “Solid-state refrigeration: A comparison of the energy performances of caloric materials operation in an caloric regenerator”. *Energy*, Vol. 165, No. Part A, pp. 439–455.

Aprea, C., Greco, A., Maiorino, A. and Masselli, C., 2019. “The use of barocaloric effect for energy saving in a domestic refrigerator with ethylene-glycol based nanofluids: A numerical analysis and a comparison with a vapor compression cooler”. *Energy*, Vol. 190, pp. 1–11.

Cui, J., Wu, Y., Muehlbauer, J., Hwang, Y., Radermacher, R., Fackler, S., Wuttig, M. and Takeuchi, I., 2012. “Demonstration of high efficiency elastocaloric cooling with large δt using niti wires”. *Applied Physics Letters*, Vol. 101, No. 7, pp. 1–4.

Greco, A., Aprea, C., Maiorino, A. and Masselli, C., 2019. “A review of the state of the art of solid-state caloric cooling processes at room-temperature before 2019”. *International Journal of Refrigeration*, Vol. 106, pp. 66–88.

Imamura, W., 2020. *Barocaloric effect in natural graphite/polydimethylsiloxane composites (in Portuguese)*. Ph.D. thesis, Faculdade de Engenheria Mecânica, Universidade Estadual de Campinas, Campinas, Brasil.

Imamura, W., Paixão, L.S., Usuda, E.O., Bom, N.M., S Gama, E.S.N.L. and Carvalho, A.M.G., 2018. “i-caloric effects: a proposal for normalization”. In *Proceedings of the 8th International Conference on Caloric Cooling - Thermag VIII*. Darnstad, Germany, pp. 179–184.

Kirsch, S.M., Welsch, F., Michaelis, N., Schmidt, M., Wieczorek, A., Frenzel, J., Eggeler, G., Schütze, A. and Seelecke, S., 2018. “Niti-based elastocaloric cooling on the macroscale: From basic concepts to realization”. *Energy Technology*, Vol. 6, No. 8, pp. 1567–1587.

Mota-Babiloni, A., Barbosa Jr., J.R. and P Makhnatch, J.A.L., 2020. “Assessment of the utilization of equivalent warming impact metrics in refrigeration, air conditioning and heat pump systems”. *Renewable and Sustainable Energy Reviews*, Vol. 128, pp. 1–15.

Papasavva, S. and Moomaw, W.R., 1998. “Life-cycle global warming impact of cfcs and cfc-substitutes for refrigeration”. *Journal of Industrial Ecology*, Vol. 1, No. 4, pp. 71–91.

Shapiro, H.N. and Moran, M.J., 2006. *Fundamentals of Engineering Thermodynamics*. 5th edition. John Wiley Sons, Inc.

Takeuchi, I. and Sandeman, K., 2015. “Solid-state cooling with caloric materials”. *Physics Today*, Vol. 68, No. 12, pp. 48–54.

Tusek, J., Engelbrecht, K., Eriksen, D., Dall’Olio, S., Tusek, J. and Pryds, N., 2016. “A regenerative elastocaloric heat pump”. *Applied Physics Letters*, Vol. 101, No. 161134, pp. 1–6.

Wang, R., Fang, S., Xiao, Y., Gao, E., Jiang, N., Li, Y., Mou, L., Shen, Y., Zhao, W., Li, S., Fonseca, A.F., Galvão, D.S., Chen, M., He, W., Yu, K., Lu, H., Wang, X., Quian, D., Aliev, A.E., Li, N., Haines, C.S., Liu, Z., Mu, J., Wang, Z., Yin, S., Lima, M.D., An, B., Liu, Z. and Baughman, R.H., 2019. “Torsional refrigeration by twisted, coiled, and supercoiled fibers”. *Science*, Vol. 366, No. 6462, pp. 216–221.

Wang, R., Zhou, X., Wang, W. and Liu, Z., 2020. “Twist-based cooling of polyvinylidene difluoride for mechanothermochromic fibers”. *Chemical Engineering Journal*, Vol. 417, No. 128060, pp. 1–9.